Wind and Structures, *Vol. 30, No. 5 (2020) 499-509*
DOI: https://doi.org/10.12989/was.2020.30.5.499

Effect of countermeasures on the galloping instability of a long-span suspension footbridge

Ruwei Ma[1,2a], Qiang Zhou[*1,2] and Mingshui Li[1,2b]

[1]*Research Centre for Wind Engineering, Southwest Jiaotong University, Chengdu, China*
[2]*Key Laboratory for Wind Engineering of Sichuan Province, Chengdu, China*

(*Received September 5, 2019, Revised January 13, 2020, Accepted March 9, 2020*)

Abstract. The aeroelastic stability of a long-span suspension footbridge with a bluff deck (prototype section) was examined through static and dynamic wind tunnel tests using a 1:10 scale sectional model of the main girder, and the corresponding aerodynamic countermeasures were proposed in order to improve the stability. First, dynamic tests of the prototype sectional model in vertical and torsional motions were carried out at three attack angles (α = 3°, 0°, -3°). The results show that the galloping instability of the sectional model occurs at α = 3° and 0°, an observation that has never been made before. Then, the various aerodynamic countermeasures were examined through the dynamic model tests. It was found that the openings set on the vertical web of the prototype section (web-opening section) mitigate the galloping completely for all three attack angles. Finally, static tests of both the prototype and web-opening sectional models were performed to obtain the aerodynamic coefficients, which were further used to investigate the galloping mechanism by applying the Den Hartog criterion. The total damping of the prototype and web-opening models were obtained with consideration of the structural and aerodynamic damping. The total damping of the prototype model was negative for α = 0° to 7°, with the minimum value being -1.07%, suggesting the occurrence of galloping, while that of the web-opening model was positive for all investigated attack angles of α = -12° to 12°.

Keywords: long-span suspension footbridge; galloping instability; web opening; Den Hartog criterion; damping

1. Introduction

Lightweight, low-damping footbridges are relatively flexible and sensitive to wind- and pedestrian-induced vibrations, which imply safety and serviceability problems. The structural characteristics of footbridges and the excitations caused by pedestrians are two significant factors that affect the dynamic behavior of footbridges and pedestrian comfort levels. Pedestrian-induced vibrations have thus been acknowledged and investigated extensively by previous studies (Fujino *et al*. 1993, Gardner-Morse and Huston 1993, Brownjohn 1997, Dallard *et al*. 2001, Živanović *et al*. 2005, Occhiuzzi *et al*. 2008, Heinemeyer *et al*. 2009, Mulas *et al*. 2018). In recent years, the popularization of footbridges with longer spans and lower weights has resulted in more flexible structures with lower natural frequencies, as well as an increased risk of resonance (Heinemeyer and Feldmann 2009, Faridani and Barghian 2012, Vladimír *et al*. 2017). Therefore, the aeroelastic performance of flexible footbridges is becoming increasingly significant, and even playing a crucial role in their dynamic design.

In the cases of common highway suspension bridges, attention has primarily been paid to their flutter instability (Zhou *et al*. 2006, Cao and Cao 2017, Li *et al*. 2018). However, for long-span footbridges with bluff decks, which are long slender bluff bodies in nature, galloping instability may become a very predominant issue.

The galloping phenomenon was first discovered by Den Hartog (1932), who introduced a very simple criterion to assess the stability of crosswind oscillations. Since then, a considerable amount of literature has been published with the aim of improving the understanding of the galloping instability of bluff bodies with basic shapes, such as circular, rectangular or square cylinders (Parkinson and Smith 1964, Novak 1972, Bearman and Luo 1988, Cheng *et al*. 2008, Tang *et al*. 2015), and power line conductors, bridge cables, hangers, etc. (MA and GU 2012, Nikitas and Macdonald 2015). Piccardo *et al*. (2011) predicted the critical galloping conditions of an inclined square cylinder based on the Den Hartog criterion. They found that yaw effects might influence the critical conditions from a quantitative point of view, but do not destroy the instability domain obtained in the classical cross-flow conditions. Tang *et al*. (2015) investigated the aeroelastic response of an inclined square cylinder in smooth flow using three-dimensional numerical simulations and reproduced the vertical bending galloping at an inclination angle of zero. Gao and Zhu (2016) studied the unsteady galloping instability of a rectangular 2:1 cylinder by measuring the nonlinear unsteady galloping force through free-vibration wind tunnel tests. They concluded that the galloping instability is governed by the nonlinear aerodynamic

*Corresponding author, Ph.D. Assistant Professor
E-mail: milan1023@gmail.com
[a]Ph.D. Student
[b]Ph.D. Professor

ISSN: 1226-6116 (Print), 1598-6225 (Online)

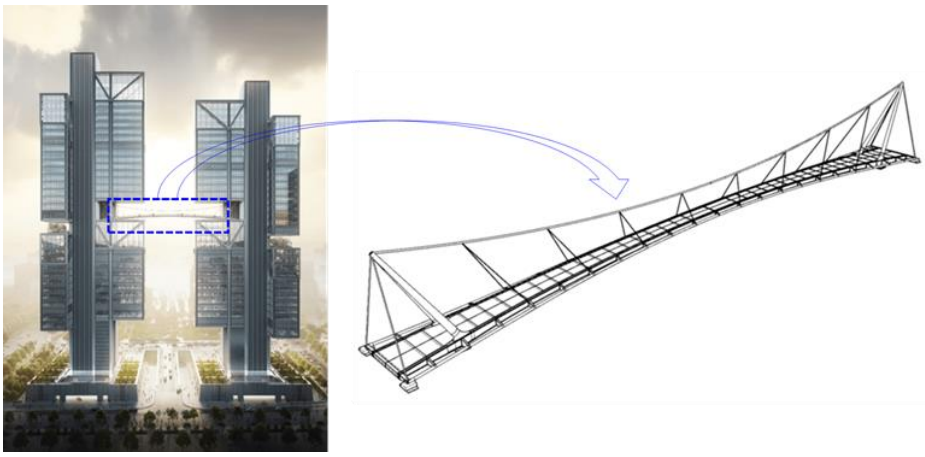

(a) Span layout

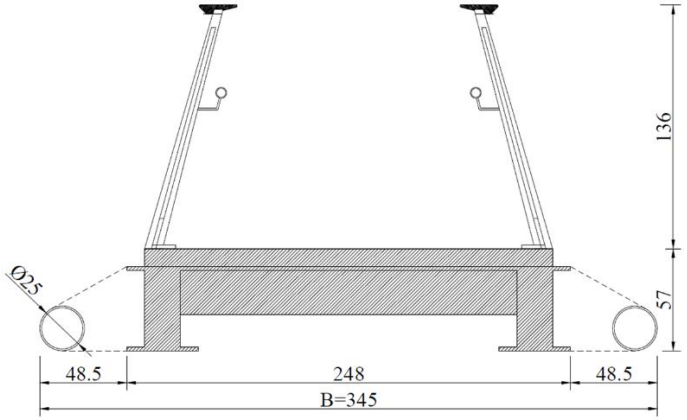

(b) Cross section of the deck (unit: cm)

Fig. 1 Schematic diagram of the suspension footbridge

damping. Chen *et al*. (2012) investigated the galloping stability of H-section booms and discussed the effect of web openings on galloping control. They confirmed the ability of web openings to improve the galloping stability. Gandia *et al*. (2014) investigated the galloping stability of porous H-section sections through a series of static and dynamic experiments and elucidated the influence of the geometrical parameters of H-section sections on the galloping stability. Li *et al*. (2017) Li *et al*. (2017) determined the galloping instability of the flat-topped main cables of a long-span suspension bridge and attributed the appearance of galloping to the negative Den Hartog coefficients. Recently, Ma *et al*. (2019) carried out a series of wind tunnel tests and pointed out that the galloping of a circular cylinder occurs via excitation and interacts with the flow regime during the transitional process.

Compared with the studies focused on the galloping instability of basic bluff bodies, little attention has been paid to that of the cross-sectional shapes of real bridges. Alonso *et al*. (2009) analyzed the galloping properties of rhomboidal and triangular cross sections through wind tunnel tests and proved that both the attack angle and section geometry have significant effects on the galloping stability. Andrianne *et al*. (2014) proposed an empirical model to describe the galloping bifurcation behavior of a bridge section, which is based on a general polynomial form proposed by Novak, but they did not put forward the countermeasure to improve the galloping stability. Buljac *et al*. (2017) studied the influence of the wind-barrier porosity and height on the galloping stabilities through wind tunnel tests of three suspension highway-bridges: the Golden Gate Bridge (USA), the Kao-Pin Hsi Bridge (Taiwan) and the Great Belt Bridge (Denmark), and found that wind barriers negligibly influence bridge susceptibility to galloping. Ge *et al*. (2002) investigated the galloping instability of the Yadagawa Bridge in Japan through both CFD computational simulations and wind tunnel tests. They discovered that aerodynamic deflectors are among the most effective measures of improving the galloping stability of certain bridges.

As summarized above, most research has focused on investigating the galloping instability of basic bluff bodies and common highway bridge sections. However, to the best of our knowledge, the galloping characteristics of long-span footbridges are seldom found in the literature, even though their galloping instability should be of great concern as their spans get longer. The motivation of the present study is thus to investigate the galloping instability and mechanism of a real long-span suspension footbridge. To achieve this, dynamic wind tunnel tests using a 1:10 section model of the main girder are carried out under three attack angles (α=+3°, 0°, -3°), and different aerodynamic

Table 1 The first eight structural vibration modes

NO.	Frequency (Hz)	Mode
1	0.823	V-S-1
2	1.207	V-A-1
3	2.262	V-S-2
4	2.486	L-S-1
5	3.498	T-S-1
6	3.635	V-A-2
7	4.926	T-A-1
8	5.357	V-S-2

S=symmetrical, A=asymmetrical, V=vertical bending, T=torsion, L=lateral bending

countermeasures are then proposed and examined. Static tests of both the prototype and web-opening models are performed to obtain the aerodynamic coefficients. Based on the quasi-steady assumption, further study is devoted to investigating the galloping mechanism by applying a modified Den Hartog criterion.

2. Experimental setup

2.1 Description of the prototype bridge

The objective bridge is a long-span suspension footbridge connecting two high-rise buildings on the southeastern coast of China. It is located at a height of 100 meters from the ground and has a main span of 76 meters, as shown in Fig. 1(a). The prototype section of the main deck is an approximately rectangular box girder which consists of a steel plate and two vertical rectangular webs on two sides. To meet the aesthetic requirements, there are two steel cylindrical structures with diameters of 25 cm at both sides of the deck, which have little effect on the structural characteristics. The overall width and height of the mid-span deck are 345 cm and 57 cm, respectively, and the pedestrian handrail is 136 cm high, as shown in Fig. 1(b).

2.2 Structural dynamic properties

In order to obtain the design parameters of the dynamic sectional model, a modal analysis was performed to determine the structural dynamic properties of the footbridge using the three-dimensional Finite Element Method (3D-FEM). This is the same method used in Zhou *et al*. (2018) for their mechanism of aerostatic instability. The structural dynamic properties characterized by natural frequencies and mode shapes were acquired and the first eight vibration modes are listed in Table 1.

Here, the vibration mode, which is defined by the mode shape of the main girder, can be divided into symmetrical and asymmetrical modes where the central axis was taken as the axis of symmetry, as shown in Fig. 2. S and A indicate the symmetrical and asymmetrical modes, respectively. The modes can also be divided into vertical, lateral and torsional modes according to the vibration direction, where V, L and T indicate the vertical, lateral and torsional modes, respectively.

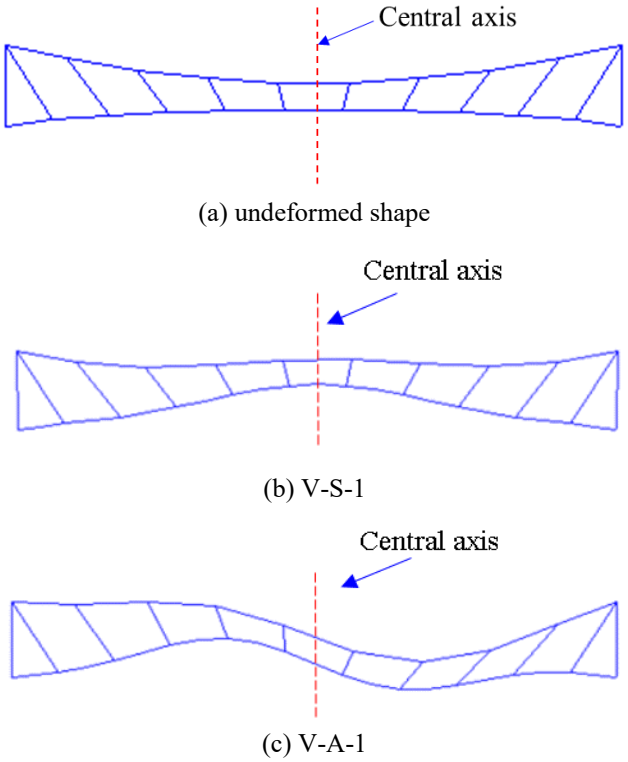

Fig. 2 The first order symmetrical and asymmetrical vertical vibration modes

2.3 Sectional model

The cross section of the footbridge is variable on its span length, as shown in Fig. 1. Thus, the deck section with the width B=3.45 m at its middle span, which was the bluffest cross-section, was selected to carry out the wind tunnel tests to maintain the stability of this footbridge. A 1:10 scale sectional model with a constant mid-span cross section was designed and had a length of 2.095 m, which maintains the aspect ratio to satisfy the required value of 3 (Sun *et al*. 2013). The entire deck model was made of wood and coated with an FRP shell to ensure its rigidity. The handrails were made of ABS. The end plates of section model is 0.550 m × 0.200 m, which is about 5 times the area of the experimental cross section.

The dynamic model system had two supports and eight tensile springs, allowed to oscillate in two degrees (vertical and torsional) of freedom, as shown in Fig. 3. In addition, two end plates were added onto the model ends to reduce the effects of the end flow and to maintain a nominally two-dimensional flow. To observe both the galloping oscillation and the vortex-induced vibration, as well as the flutter instability, a frequency scale of 1.6 based on the first vertical bending mode (V-S-1) was chosen for the dynamic sectional model tests. The physical properties of the dynamic sectional model are presented in Table 2. The blockage ratio for this study is 2.6%, which is less than the suggested value of 5% (Choi and Kwon 1998).

In addition, the static sectional model, which uses the

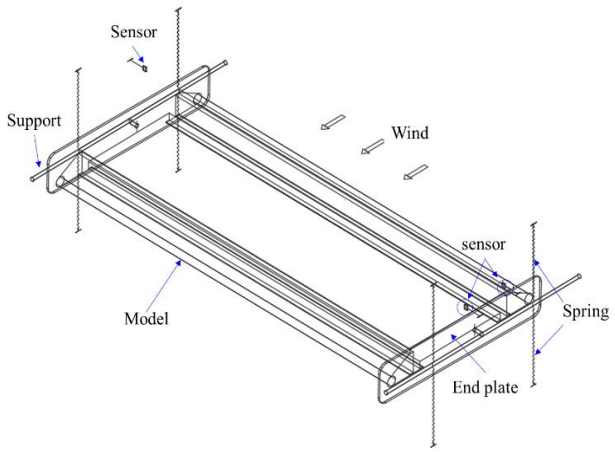

Fig. 3 Schematic diagram of the dynamic sectional model

Table 2 Physical properties of dynamic sectional model

Items	Unit	Prototype	Scale ratio	Model
Length (L)	m	20.95	1/10	2.095
Width (B)	m	3.45	1/10	0.345
Height (H)	m	0.57	1/10	0.057
Mass/meter	kg/m	2613.7	$1/10^2$	26.137
Inertia/meter	kg·m	5911.4	$1/10^4$	0.591
Vertical natural frequency (f_v)	Hz	0.823	/	1.324
Torsional natural frequency (f_t)	Hz	3.498	/	5.679
Frequency ratio	f_t/f_v	4.250	1	4.289
Vertical damping ratio	%	0.35	1	0.340
Torsional damping ratio	%	0.35	1	0.280
Wind velocity scale	/	/	6.16	/

same geometric scale as the dynamic sectional model, was connected to a force balance system to measure the drag, lift and pitch forces.

2.4 Test conditions

The dynamic and static sectional model tests were carried out in the second test section of the XNJD-1 wind tunnel at Southwest Jiaotong University, which is of the horizontally closed-circuit type and has a working section of 2.4 m in width, 2.0 m in height and 16.0m in length. The wind velocity in this working section can be adjusted continuously from 0.5 m/s to 22.0 m/s. All the tests were conducted in a smooth flow with a background turbulence intensity of less than 1%.

For the dynamic tests, the attack angles were set as +3°, 0° and -3°. As shown in Fig. 3, the vertical and torsional displacement responses of the model can be measured by two separate laser displacement sensors, which have a measuring range of 200 mm and a static measurement accuracy of 40μm with a sampling frequency of 1kHz.

For the static tests, the model was connected to the force balance system, which can range from -20° to +20°. The design load of the three-component strain balance is as follows: drag force F_D = 500N, lift force F_L = 1200N and pitch moment M = 120N·m. The static tests were conducted with attack angles ranging from -12° to +12° at increments of $\Delta\alpha$=1°. To ensure the reliability and accuracy of the results, all the static tests were performed at a high wind velocity of 15 m/s, which can maintain a better signal-to-noise ratio.

3. Results and Discussion

3.1 Galloping performance of the prototype section

Fig. 4(a) and (b) present the dimensionless root-mean-square (RMS) values of the amplitudes of the vertical and torsional vibrations for the prototype section at various reduced wind velocities, respectively, where the amplitude of vertical displacement, as well as the RMS values σ_v and σ_t, has been normalized by the deck width B. It can be found that vertical oscillations with significant amplitudes occur at both attack angles of α = +3° and 0° as the wind velocity exceeds the critical values, U/fB = 17.2 and 21.8, respectively. This is followed by a rapid increase with increasing wind velocity. Here, U is the oncoming wind velocity, f is the measured vertical frequency, and B is the deck width. However, as shown in Fig. 4(b), the amplitude of the torsional vibration remains zero with the increase of the reduced wind velocities, which illustrates that there is no torsional vibration for all three attack angles. It can be concluded that the vertical galloping instability of the main girder, rather than the flutter instability, occurs at α = +3° and 0° as the reduced wind velocities are larger than 17.2 and 21.8, respectively. To our knowledge, this is the first case of galloping instability in a long-span footbridge. It suggests that the particular attention should be paid to the aeroelastic instability of a long-span footbridge in addition to its pedestrian-induced vibration problem. As for the case of α=-3°, no obvious vertical oscillation was found for all reduced wind velocities. The vertical amplitude at the maximum U/fB = 31.9 remained very small, as shown in Fig. 4a. This means that no galloping instability occurs in the range of the studied wind velocities at α = -3°.

Figs. 5 and 6 show the time histories and spectra of vertical vibrations at various reduced wind velocities for α = 0° and +3°, respectively. It can clearly be seen that the vertical vibration shows approximately harmonic sinusoidal motion as the galloping occurs, and its amplitude remains almost unchanged for all the studied wind velocities, although the amplitude of the vertical vibration increases approximately linearly with the increasing wind velocity, as shown in Fig. 4(a). However, the dominant frequency of the galloping oscillation remains unchanged with increasing wind speed, and is almost identical to the vertical natural frequency f_v of the dynamic sectional model system. This indicates that the effect of the aerodynamic stiffness of the main deck on the galloping instability is very small compared to that of the aerodynamic damping, which is similar to the conclusion reached by Gao and Zhu (2016) for a rectangular section. In other words, the aerodynamic damping plays a dominant role in the galloping instability of this kind of bluff section, and attention should be paid to

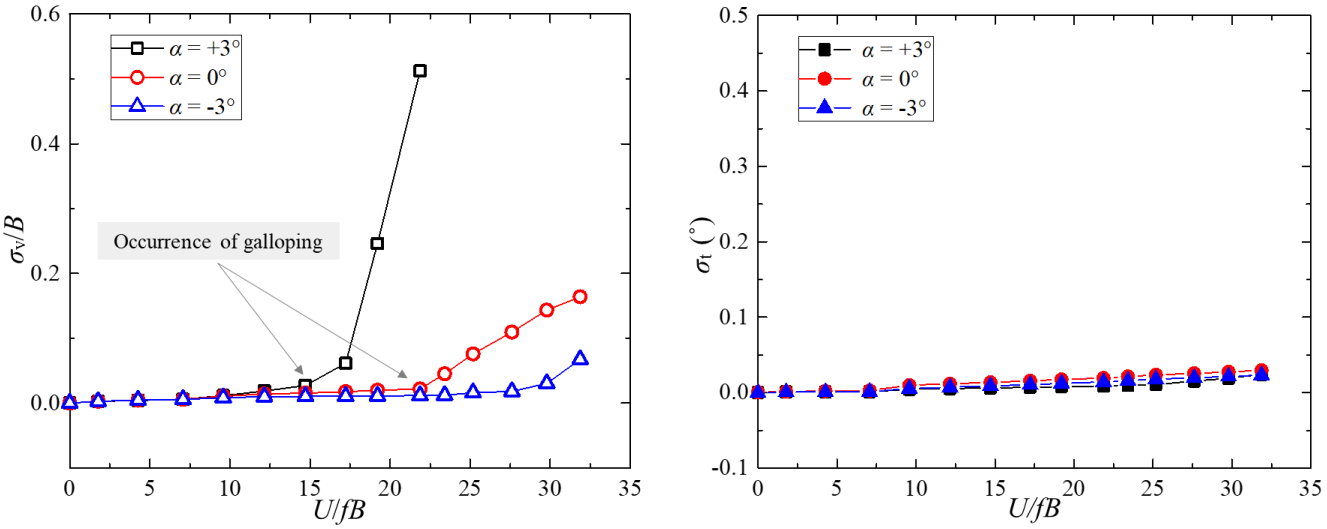

(a) Vertical response (b) Torsional response

Fig. 4 Variation of the vertical and torsional vibrations of prototype section with reduced wind velocity

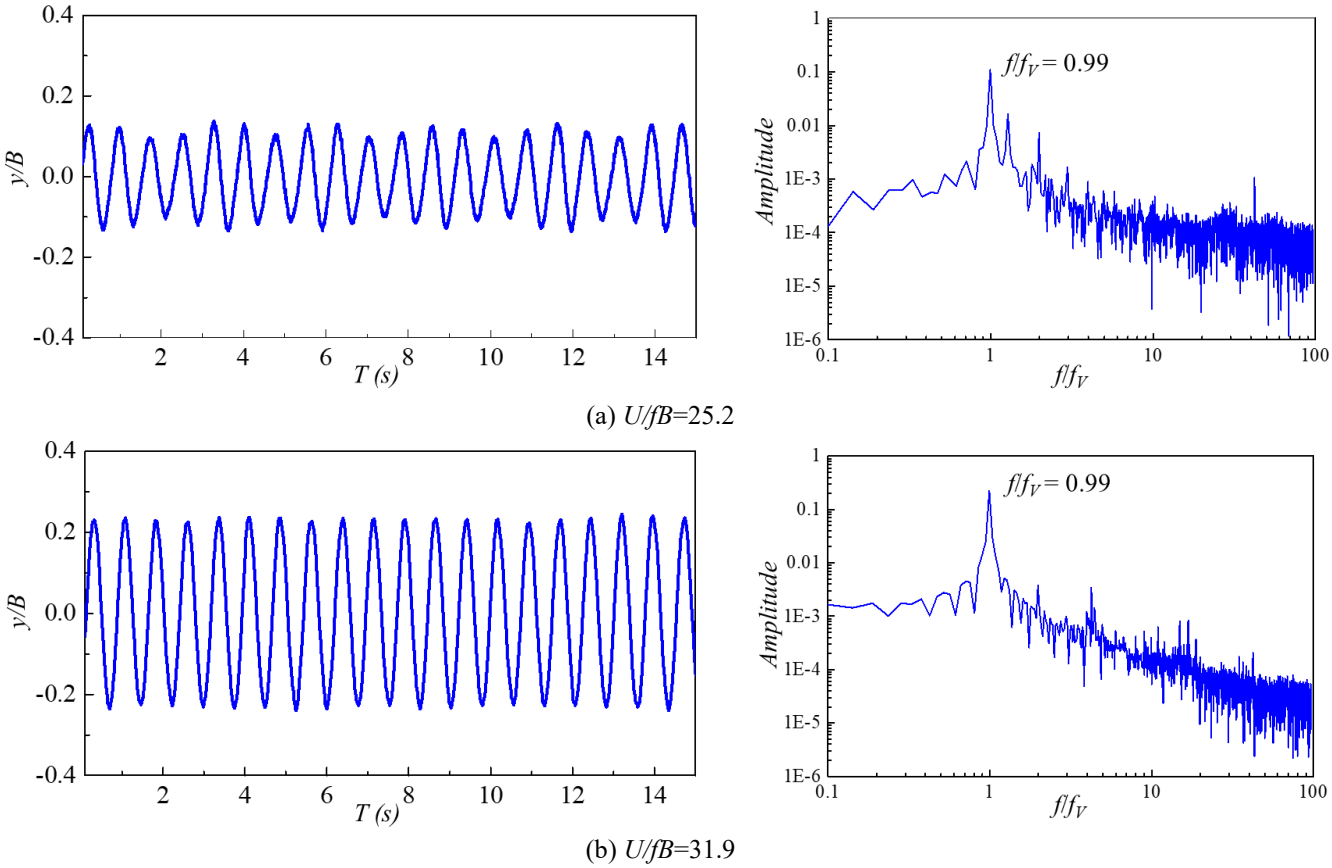

(a) *U/fB*=25.2

(b) *U/fB*=31.9

Fig. 5 Time history and spectrum of vertical vibration at various reduced wind velocities (α=0°)

the aerodynamic damping to investigate the mechanism of galloping, which will be discussed later.

3.2 Aerodynamic countermeasures

The galloping instability of the prototype footbridge can be improved structurally, aerodynamically and mechanically. As a substantial change in the cross-sectional configuration of the main girder is not practical in the case of this bridge, we have to seek aerodynamic or mechanical countermeasures, such as the installation of tuned mass dampers. The aerodynamic countermeasures were chosen due to their lower cost and manufacturing convenience. As mentioned in previous studies (Ge *et al*. 2002, Ma *et al*. 2005, Sarwar and Ishihara 2010, Zhou *et al*. 2015, Larsen 2017, Li *et al*. 2018), aerodynamic countermeasures, such

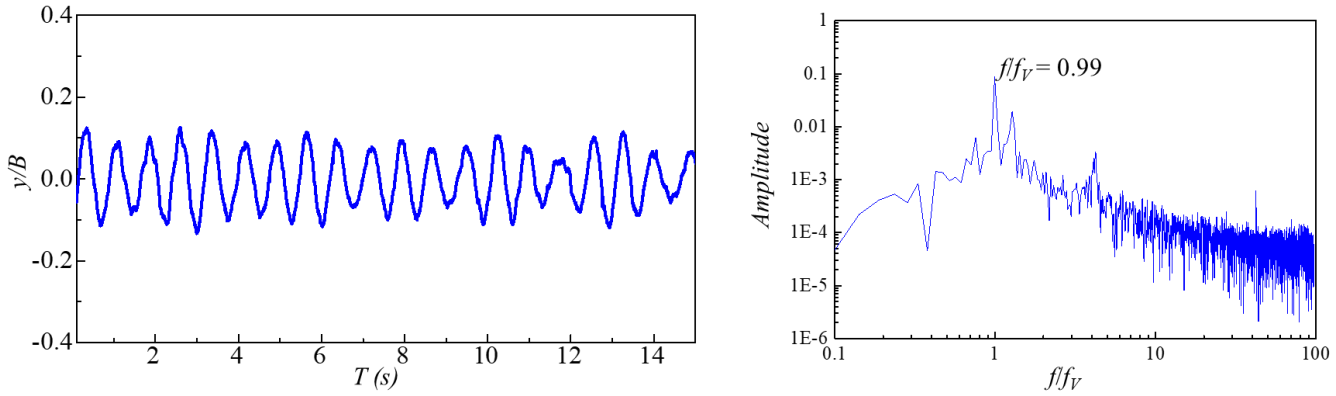

(a) U/fB = 17.2

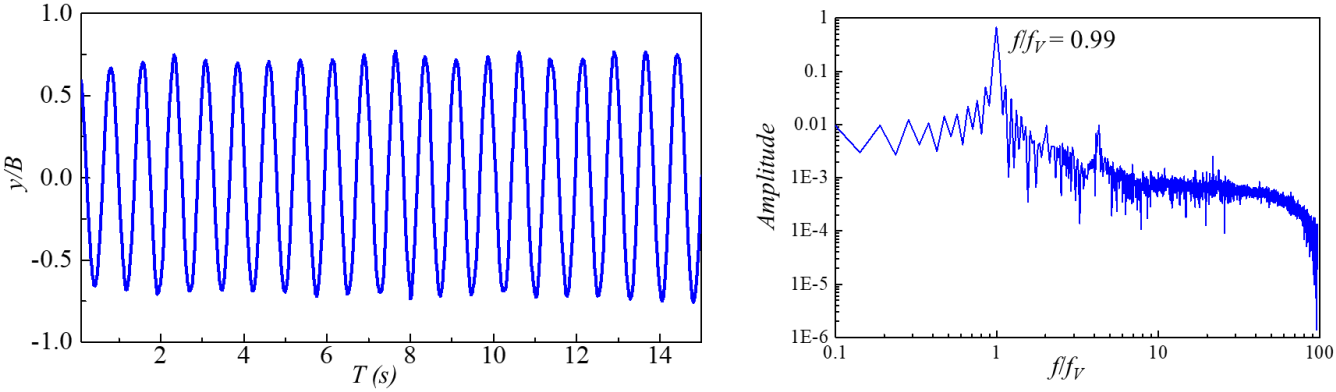

(b) U/fB = 21.9

Fig. 6 Time history and spectrum of vertical vibration at various reduced wind velocities (α=+3°)t

as fairings, flaps, corner deflectors, splitter plates, soffit plates, baffle plates, fins, spoilers and so on, have been extensively applied to improve the flutter stability or mitigate the vortex-induced vibration response of long-span bridges. Similarly, in the present study, eight aerodynamic countermeasures referred to as A - H were designed to improve the galloping stability of this footbridge, as shown in Figs. 7 - 9.

According to the configuration, the aerodynamic countermeasures were divided into three groups. Group one, consisting of measures A - D, is characterized by additional deflectors, as shown in Fig. 7(a) - 7(d). The two cylindrical structures on both sides are entangled with a helical cable in measure A to reduce the influence of the flow around the cylinder. Measure B consists of installing two 10-cm horizontal deflectors on the top side edge of the main deck. Measure C involves sealing the upper side of the gap between the cylindrical structure and the bridge deck using two deflectors, while measure D involves sealing both the upper and lower sides of the gap with deflectors. Group two, consisting of measures E - G, is characterized by the combination of deflectors and stabilizers, as shown in Fig. 8(a) - 8(c). Measure E adds a central stabilizer with a height of 30 cm based on measure C. Measure F adds two vertical stabilizers with heights of 20 cm on the lower inner side-corner of the main deck based on measure C. In measure G, discontinuous grilles and two 20-cm vertical stabilizers are installed in the gap and the lower inner side-corner, respectively. Group three consists only of measure F, where the openings of the rectangular holes with 3-cm chamfers were set on the vertical web of the main deck, as shown in Fig. 9. We have also named the cross section using measure H the web-opening section.

Fig. 10(a) compares the vertical vibration response of the sections with countermeasures in group one with those of the prototype section. It is found that measures A, B and D worsen the galloping instability, as the severe vertical vibration occurs at a lower wind velocity than that of the prototype section. As for measure C, the vertical vibration is completely mitigated at α = +3°, which indicates the galloping stability is improved. However, the critical wind velocity of the galloping instability at α = 0° becomes lower than that of the prototype section. Measure D, which can sharpen the prototype section, is often taken to improve the flutter stability of the common long-span highway bridge. However, the effect of measure D is totally negative for galloping stability of this kind long-span footbridge, where the dimensionless critical wind velocities Uf/B decrease dramatically to 7.06 and 7.07 at α = +3° and 0°, respectively. It means that setting deflectors fails to improve the galloping stability for all studied attack angles, although it has a positive effect at certain specific attack angles. It also suggests that the attention should be paid to galloping as choosing the countermeasure to improve the flutter stability. As shown in Fig. 10(b), measure G, which substitutes discontinuous grilles for the sealing deflectors seen in measure F, mitigated the vertical vibrations for α = +3° and α = 0°, while vertical galloping instability also

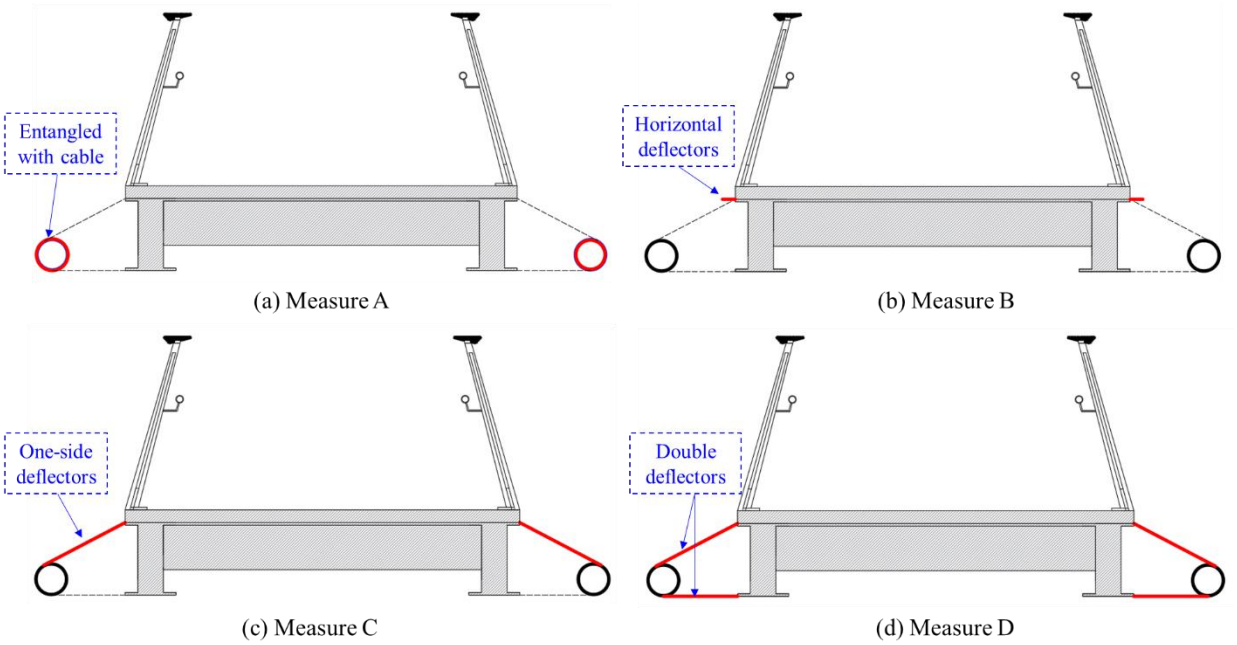

Fig. 7 Schematic diagram of countermeasures in Group one

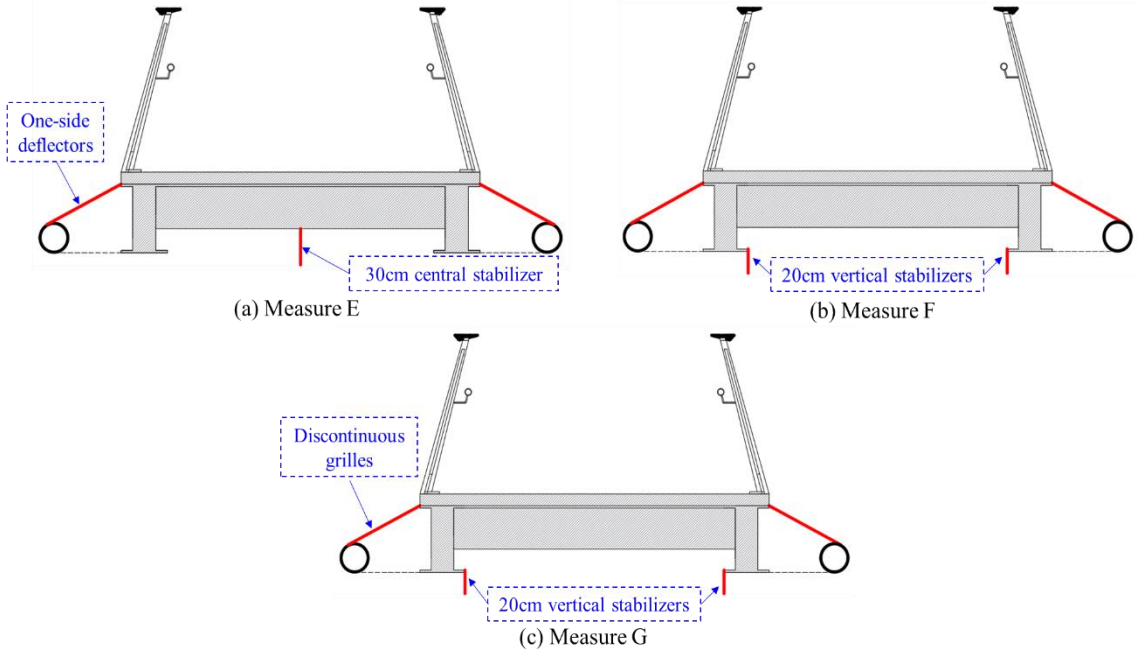

Fig. 8 Schematic diagram of countermeasures in Group two

occurred for α = -3° at a high wind velocity. In contrast to the above-mentioned countermeasures, measure F adopts the idea of subtraction and sets the openings on the vertical web, which is similar to the measure applied in the previous studies (Ma *et al*. 2005, Chen *et al*. 2012). From Fig. 10(c), it can be observed that the vertical vibrations are completely suppressed by the application of web-openings for all the studied attack angles. The web openings show the most positive effect ~~in~~ on stabilizing the galloping of this sectional model. In addition, the countermeasure of web openings is the best choice from an economic perspective due to the fact that it requires less material consumption and a shorter construction period.

3.3 Galloping mechanism

The galloping of slender structures is a kind of bending, wind-induced, self-excited and unstable oscillation (Chen *et al*. 2012). According to the quasi-steady theory of galloping, the galloping instability for a certain section can Be evaluated by the Den Hartog coefficient proposed by Den Hartog (1932) as follows

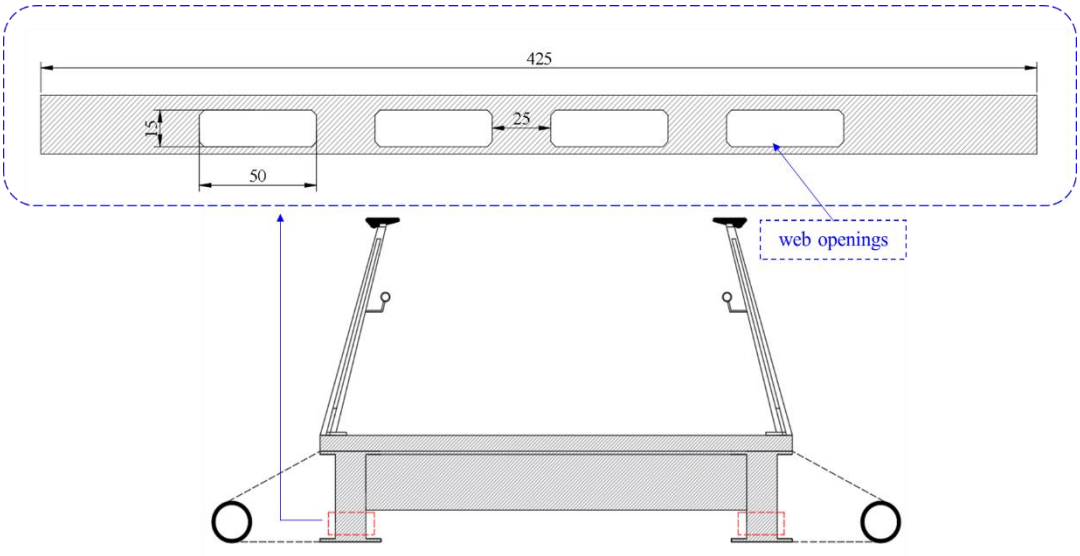

Fig. 9 Schematic diagram of web openings (Measure H)

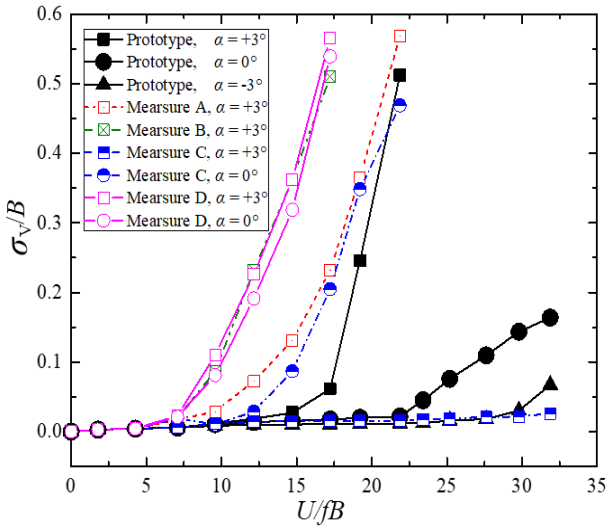

(a) Effects of the countermeasures of Group one

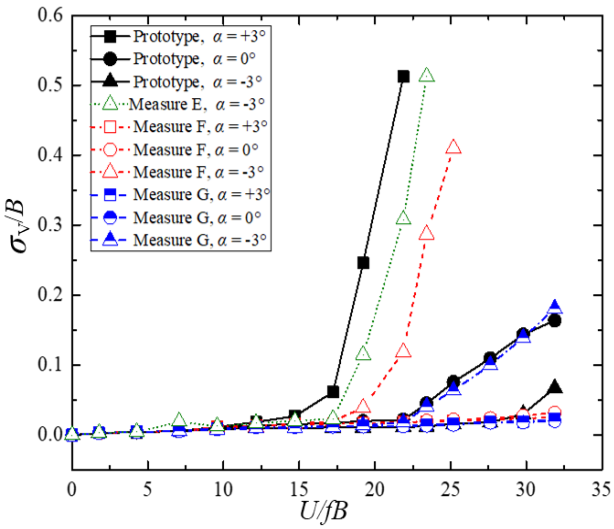

(b) Effects of the countermeasures of Group two

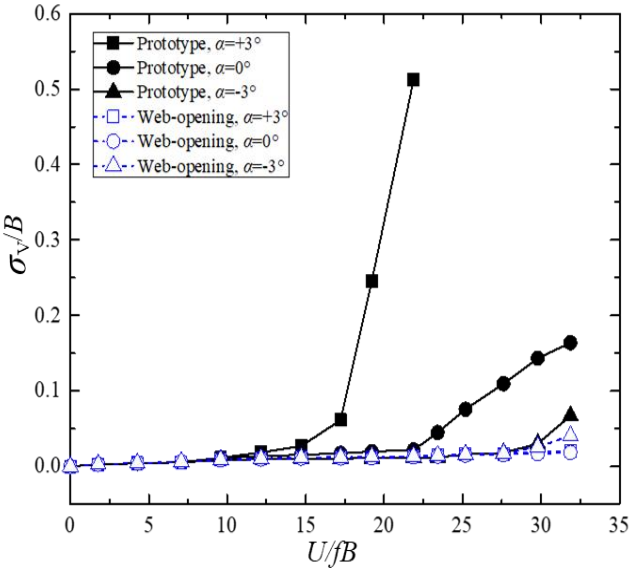

(c) Effects of web openings

Fig. 10 Effects of the countermeasures on the vertical galloping

$$s = \frac{dC_L}{d\alpha} + C_D \tag{1}$$

where C_D and C_L are the drag and lift coefficients, respectively. Thus, the Den Hartog coefficient equals the sum of the drag coefficient and the derivative of the lift coefficient with the attack angle. The necessary criterion for galloping to occur is $s < 0$, which is based on the quasi-steady state assumption and linearization, and is extensively applied for engineering purposes.

To evaluate the Den Hartog coefficient, the sectional wind tunnel tests of prototype sectional model and web-opening sectional model connecting to a high-frequency force balance were carried out in uniform flow with the wind velocity of 15 m/s. The steady aerodynamic lift coefficient C_L and drag coefficient C_D at attack angles from -12° to 12°, with the step increment of 1°. The C_D and C_L were calculated by the following equations

$$C_D(\alpha) = F_D(\alpha) / (\frac{1}{2}\rho U^2 BL) \tag{2}$$

$$C_L(\alpha) = F_L(\alpha) / (\frac{1}{2}\rho U^2 BL) \tag{3}$$

where ρ is the air density, U is the oncoming flow velocity (15m/s in the present experiments) and $F_D(\alpha)$ and $F_L(\alpha)$ are respectively the drag force and the lift force as a function of the attack angle α. The measured drag and lift coefficients for the prototype section and the web-opening section are shown in Fig. 11, wherein the open- and solid-symbols represent the aerodynamic coefficients of the prototype and web-opening sections, respectively. The values of C_D for both sections are closely aligned. However, a negative slope for C_L is observed in the range of α = -7° to 7°, particularly in the range of -3° to 7° for the prototype section, which indicates a worsening galloping instability performance. As for the web-opening section, the negative C_L slope apparently decreases due to the web openings, which could also be the cause of the different galloping behaviors of the two sections, as discussed below.

Fig. 12 compares the Den Hartog coefficients of the prototype section and the web-opening section at different attack angles, where a significant disparity can obviously be found. As for the prototype section, the Den Hartog coefficient decreases rapidly from α = -12° to 5°, after which it begins to increase dramatically. The values of the Den Hartog coefficient are negative in the range of -2° ≤ α ≤ 7°, which suggests that galloping instability may occur in the range of α = -2° to 7° according to the quasi-steady theory. This aligns well with the results of the dynamic sectional model tests for the prototype section, where galloping did occur at α = 0° and +3°. As for the web-opening section, the Den Hartog coefficient increases at most attack angles compared to that of the prototype section, which indicates that the galloping stability of the web-opening section is significantly improved. However, the Den Hartog coefficient of the web-opening section is slightly less than zero from α = -1° to 1°, which is inconsistent with the results obtained from the previous dynamic sectional model tests, where galloping instability did not occur within the studied

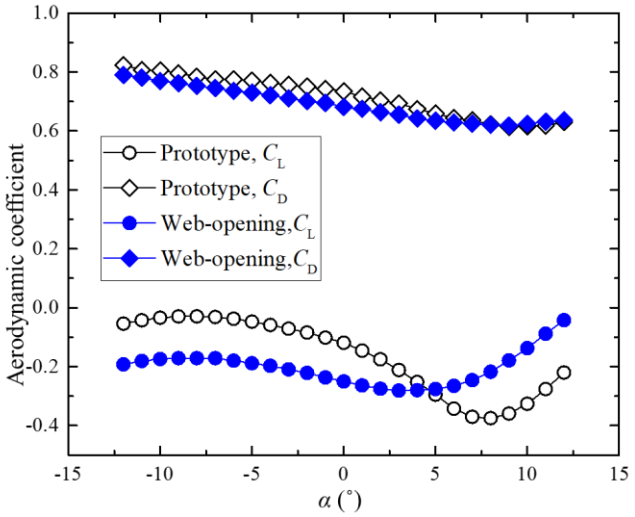

Fig. 11 Drag and lift coefficients with different attack angles

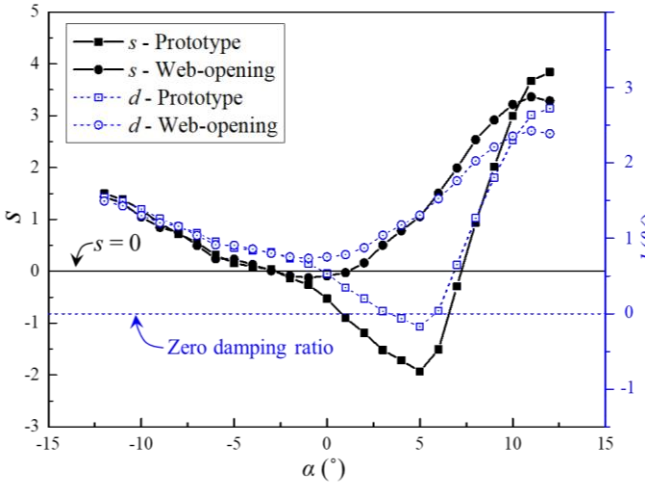

Fig. 12 Den Hartog coefficients (S) and total damping ratio (d, %) at different attack angles

wind velocity range. The main reason for this inconsistency between the theoretical analysis and experimental results is a lack of consideration of the structural damping.

In this study, a modified galloping-analysis method, taking both aerodynamic and structure damping into consideration, was adopted based on the Den Hartog coefficient. According to the equation of the classically heaving DOF (y)

$$m(\ddot{y} + 2\xi\omega\dot{y} + \omega^2 y) = F_y(\alpha) \tag{4}$$

where m is the mode mass, ξ is dumping ratio, ω is the structural circular frequency, and $F_y(\alpha)$ is the quasi-steady aerodynamic force.

$F_y(\alpha)$ can be derived as follows

$$F_y(\alpha) = \frac{1}{2}\rho U^2 B(C_D \sin\alpha + C_L \cos\alpha) \tag{5}$$

As the section is oscillating in the y-direction with velocity $\dot{y}$, there will be a reduction in the apparent angle

of attack of the flow by $\dot{y}/U$, or an increase in angle of attack by $-\dot{y}/U$ (Holmes 2018).

Assuming the angle of attack to be small and hence,

$$F_y(\alpha) = -\frac{1}{2}\rho U^2 B\left(\frac{\mathrm{d}C_L}{\mathrm{d}\alpha} + C_D\right)\cdot\frac{\dot{y}}{U} \tag{6}$$

Substituting Eq. (6) into Eq. (4), we obtain

$$m\ddot{y} + [2\xi\omega m + \frac{1}{2}\rho UB(\frac{dC_L}{d\alpha} + C_D)]\dot{y} + \omega^2 y = 0 \tag{7}$$

Hence the total damping with consideration of both the structural and aerodynamic damping can be expressed as below

$$d = 4\pi\xi fm + \frac{1}{2}\rho UB(\frac{dC_L}{d\alpha} + C_D) \tag{8}$$

where the circular frequency ω is expressed by $\omega=2\pi f$. In addition, as mentioned above, the galloping instability of this type of bluff section is mainly affected by the aerodynamic damping. Thus, the total damping d was applied to investigate the galloping mechanism.

Fig. 12 also presents the variation of the total damping d of both prototype and web-opening sections with various attack angles at U/fB = 31.9, which corresponds to the maximum vibration amplitude in the dynamic sectional model tests. The change of the total damping with respect to the attack angle is consistent with that of the Den Hartog coefficient because the structural damping for different attack angles is approximately the same. From Fig. 12, it can be found that the total damping of the prototype model is negative for α = 0° to 7°, with the minimum value being -1.07%, indicating the occurrence of galloping, and the critical wind velocity Uf/B is 17.0 at α = +3° estimated by the modified Den Hartog criterion. These align well with the previous dynamic sectional test results. It means the quasi-stationary hypothesis seems still effectively as the beginning of galloping. However, for the web-opening section, the total damping is positive for all investigated attack angles of α = -12° to 12°, which shows that the structure is stable and free of the galloping problem. This observation is also consistent with the previous experimental results.

5. Concluding Remarks

A series of static and dynamic wind tunnel tests using a 1:10 scale sectional model was conducted to investigate the galloping instability of a long-span suspension footbridge. Various aerodynamic countermeasures were proposed and their functionality was examined through the dynamic model tests. The galloping mechanism was investigated using a modified Den Hartog criterion.

The dynamic experiments concerning the prototype section model in vertical and torsional motions were carried out with three attack angles (α = +3°, 0°, -3°). The galloping instability of the prototype section occurred at α=+3° and 0°, which has not been previously observed in the literature. The vertical galloping amplitude increases approximately linearly with the increasing of the wind velocity, while the frequency of the galloping oscillation remains unchanged and is almost identical to the vertical natural frequency of the dynamic sectional model system. This indicates that the aerodynamic damping, rather than the aerodynamic stiffness, plays a decisive role in the galloping of this type of bluff section.

Various aerodynamic countermeasures, including adding horizontal deflectors on the top corner, adding vertical stabilizers on the bottom plate and setting perforations on the vertical web, were proposed to improve the bridge stability. Their functionality was examined through the dynamic model tests. The results show that setting web openings can improve the galloping instability of the main girder of the long-span footbridge for all three attack angles.

A modified galloping-analysis method based on the Den Hartog criterion, which considers both aerodynamic damping and structure damping, is applied to investigate the galloping mechanism of the prototype and web-opening sections. It was found that the total damping of the prototype model is negative for α = 0° to 7°, with the minimum value being -1.07%, suggesting the occurrence of galloping. Those of the web-opening model are positive for all investigated attack angles of α = -12° to 12°. These analytical results are consistent with the previous experimental ones. It can be concluded that the total damping, with consideration of the aerodynamic and structural damping, can be taken as the criterion for the analysis of the galloping performance of a long-span footbridge with a bluff cross section. It also suggests that the quasi-stationary hypothesis seems still effectively as the beginning of galloping.

Acknowledgements

This research was funded in part by the Natural Science Foundation of China (NSFC, No. 51708462, 51878580) and the Fundamental Research Funds for Key Laboratory of Wind-Resistant Technology for Bridge Structures (NO. KLWRTBMC18-04).

References

Alonso, G., Valero, E. and Meseguer, J. (2009), "An analysis on the dependence on cross section geometry of galloping stability of two-dimensional bodies having either biconvex or rhomboidal cross sections", *European J. Mech.-B/Fluids*., **28**(2), 328-334. https://doi.org/10.1016/j.euromechflu.2008.09.004.

Andrianne, T. and Dimitriadis, G. (2014), "Empirical modelling of the bifurcation behaviour of a bridge deck undergoing across-wind galloping", *J. Wind Eng. Ind. Aerod*., **135**, 129-135. https://doi.org/10.1016/j.jweia.2014.10.007.

Bearman, P. and Luo, S. (1988), "Investigation of the aerodynamic instability of a square-section cylinder by forced oscillation", *J. Fluid. Struct*., **2**(2), 161-176. https://doi.org/10.1016/S0889-9746(88)80017-3.

Brownjohn, J.M.W. (1997), "Vibration characteristics of a suspension footbridge", *J. Sound Vib*., **202**(1), 29-46. https://doi.org/10.1006/jsvi.1996.0789.

Buljac, A., Kozmar, H., Pospisil, S. and Machacek, M. (2017), "Flutter and galloping of cable-supported bridges with porous wind barriers", *J. Wind Eng. Ind. Aerod*., **171,** 304-318. https://doi.org/10.1016/j.jweia.2017.10.012.

Cao, S. and Cao, J. (2017), "Toward better understanding of turbulence effects on bridge aerodynamics", *Front. Built Environ*., **3** 72.

Chen, Z.Q., Liu, M.G., Hua, X.G. and Mou, T.M. (2012), "Flutter, galloping, and vortex-induced vibrations of H-section hangers", *J. Bridge Eng*., **17**(3), 500-508. https://doi.org/10.1016/j.jweia.2017.10.012.

Cheng, S., Larose, G.L., Savage, M.G., Tanaka, H. and Irwin, P.A. (2008), "Experimental study on the wind-induced vibration of a dry inclined cable-Part I: Phenomena", *J. Wind Eng. Ind. Aerod*., **96**(12), 2231-2253. https://doi.org/10.1016/j.jweia.2008.01.008.

Choi, C.K. and Kwon, D.K. (1998), "Wind tunnel blockage effects on aerodynamic behavior of bluff body", *Wind Struct. Int. J*., **1**(4), 351-364.

Dallard, P., Fitzpatrick, T., Flint, A., Low, A., Smith, R.R., Willford, M. and Roche, M. (2001), "London Millennium Bridge: pedestrian-induced lateral vibration", *J. Bridge Eng*., **6**(6), 412-417. https://doi.org/10.1061/(ASCE)1084-0702(2001)6:6(412).

Den Hartog, J. (1932), "Transmission line vibration due to sleet", *Transactions Amer. Institute Electrical Eng*., **51**(4), 1074-1076. https://doi.org/10.1109/T-AIEE.1932.5056223.

Faridani, H.M. and Barghian, M. (2012), "Improvement of dynamic performances of suspension footbridges by modifying the hanger systems", *Eng. Struct*., **34**, 52-68. https://doi.org/10.1016/j.engstruct.2011.09.025.

Fujino, Y., Pacheco, B.M., Nakamura, S.I. and Warnitchai, P. (1993), "Synchronization of human walking observed during lateral vibration of a congested pedestrian bridge", Earthquake Engineering & Structural Dynamics. 22(9), 741-758.

Gandia, F., Meseguer, J. and Sanz-Andres, A. (2014), "Static and dynamic experimental analysis of the galloping stability of porous H-section beams", *Sci. World J*., **2014**, 746826. https://doi.org/10.1155/2014/746826.

Gao, G. and Zhu, L. (2016), "Measurement and verification of unsteady galloping force on a rectangular 2: 1 cylinder", *J. Wind Eng. Ind. Aerod*., **157**, 76-94. https://doi.org/10.1016/j.jweiar.2016.08.004.

Gardner-Morse, M.G. and Huston, D.R. (1993), "Modal identification of cable-stayed pedestrian bridge", *J. Struct. Eng*., **119**(11), 3384-3404. https://doi.org/10.1061/(ASCE)0733-9445(1993)119:11(3384).

Ge, Y., Lin, Z., Cao, F., Pang, J. and Xiang, H. (2002), "Investigation and prevention of deck galloping oscillation with computational and experimental techniques", *J. Wind Eng. Ind. Aerod*., **90**(12-15), 2087-2098. https://doi.org/10.1016/S0167-6105(02)00326-4.

Heinemeyer, C. and Feldmann, M. (2009), "European design guide for footbridge vibration", CRC Press.

Heinemeyer, C., Butz, C., Keil, A., Schlaich, M., Goldack, A., Trometer, S., Lukic, M., Chabrolin, B., Lemaire, A. and Martin, P.O. (2009), "Design of leightweight footbridges for human induced vibrations".

Holmes, J.D. (2018), "Wind loading of structures", CRC Press.

Larsen, A. (2017), "Aerodynamics of large bridges", Routledge.

Li, M., Sun, Y., Jing, H. and Li, M. (2018), "Vortex-induced vibration optimization of a wide streamline box girder by wind tunnel test", *KSCE J. Civil Eng*., **22**(12), 5143-5153.

Li, S., An, Y., Wang, C. and Wang, D. (2017), "Experimental and numerical studies on galloping of the flat-topped main cables for the long span suspension bridge during construction", *J. Wind Eng. Ind. Aerod*., **163**, 24-32. https://doi.org/10.1016/j.jweia.2017.01.012.

Li, Z., Zhou, Q., Liao, H. and Ma, C. (2018), "Numerical studies of the suppression of vortex-induced vibrations of twin box girders by central grids", *Wind Struct*., **26**(5), 305-315. https://doi.org/10.12989/was.2018.26.5.305.

Ma, C.M., Liao, H.L., Zheng, S.X. and Li, J.S. (2005), "Wind tunnel experiment on the aerodynamic performances of H-shaped booms", *Zhongguo Tiedao Kexue*, **26**(4), 42-46.

Ma, W., Liu, Q. and Matsumoto, M. (2019), "Excitation of the large-amplitude vibrations of a circular cylinder under normal wind conditions in the critical Reynolds number range", *J. Fluid. Struct*., **84**, 318-328. https://doi.org/10.1016/j.jfluidstructs.2018.11.008.

MA, W.Y. and GU, M. (2012), "Galloping instability of two degree of freedom of iced conductor with swing", *Eng. Mech*., **1**(30).

Mulas, M.G., Lai, E. and Lastrico, G. (2018), "Coupled analysis of footbridge-pedestrian dynamic interaction", *Eng. Struct*., **176**(1), 127-142. https://doi.org/10.1016/j.engstruct.2018.08.055.

Nikitas, N. and Macdonald, J. (2015), "Aerodynamic forcing characteristics of dry cable galloping at critical Reynolds numbers", *European J. Mech.-B/Fluids*, **49**(Part A), 243-249. https://doi.org/10.1016/j.euromechflu.2014.09.005.

Novak, M. (1972), "Galloping oscillations of prismatic structures", *J. Eng. Mech*., **98**(1), http://worldcat.org/issn/07339399.

Occhiuzzi, A., Spizzuoco, M. and Ricciardelli, F. (2008), "Loading models and response control of footbridges excited by running pedestrians", *Struct. Control Health Monit*., **15**(3), 349-368. https://doi.org/10.1002/stc.248.

Parkinson, G. and Smith, J. (1964), "The square prism as an aeroelastic non-linear oscillator", *Quarterly J. Mech. Appl. Mathe*., **17**(2), 225-239.

Piccardo, G., Carassale, L. and Freda, A. (2011), "Critical conditions of galloping for inclined square cylinders", *J. Wind Eng. Ind. Aerod*., **99**(6-7), 748-756. https://doi.org/10.1016/j.jweia.2011.03.009.

Sarwar, M.W. and Ishihara, T. (2010), "Numerical study on suppression of vortex-induced vibrations of box girder bridge section by aerodynamic countermeasures", *J. Wind Eng. Ind. Aerod*., **98**(12), 701-711.

Sun, Y., Li, M. and Liao, H. (2013), "Investigation on vortex-induced vibration of a suspension bridge using section and full aeroelastic wind tunnel tests", *Wind Struct*., **17**(6), 565-587. https://doi.org/10.12989/was.2013.17.6.565.

Tang, Y., Zheng, S. and Li, M. (2015), "A numerical investigation on galloping of an inclined square cylinder in a smooth flow", *J. Wind Eng. Ind. Aerod*., **144**, 165-171. https://doi.org/10.1016/j.jweia.2015.03.008.

Vladimír, Š., Michal, P. and Tomáš, P. (2017), "A Dynamic Analysis of the Cable-Stayed Footbridge in Čelákovice Town", *Procedia Eng*., **199**, 2877-2882. https://doi.org/10.1016/j.proeng.2017.09.582.

Zhou, Q., Liao, H. and Wang, T. (2018), "Numerical study on aerostatic instability modes of the double-main-span suspension bridge", *Shock Vib*., 2018. https://doi.org/10.1155/2018/7458529.

Zhou, Z., Chen, A. and Xiang, H. (2006), "On the mechanism of torsional flutter instability for 1st Tacoma Narrow Bridge by discrete vortex method", *CWE*. 505-508.

Zhou, Z., Yang, T., Ding, Q. and Ge, Y. (2015), "Mechanism on suppression in vortex-induced vibration of bridge deck with long projecting slab with countermeasures", *Wind Struct*., **20**(5), 643-660. https://doi.org/10.12989/was.2015.20.5.643.

Živanović, S., Pavic, A. and Reynolds, P. (2005), "Vibration serviceability of footbridges under human-induced excitation: a literature review", *J. Sound Vib*., **279**(1-2), 1-74.

AM